Songklanakarin J. Sci. Technol.
41 (5), 1059-1068, Sep. – Oct. 2019

http://www.sjst.psu.ac.th

Original Article

An evaluation of thermal effects on behavior of a concrete arch dam

Kiet Anh Bui[1*], Pakawat Sancharoen[2], Ganchai Tanapornraweekit[2], Somnuk Tangtermsirikul[1], and Pruettha Nanakorn[1]

[1] *School of Civil Engineering and Technology, Sirindhorn International Institute of Technology, Thammasat University, Khlong Luang, Pathum Thani, 12120 Thailand*

[2] *Construction and Maintenance Technology Research Center, School of Civil Engineering and Technology, Sirindhorn International Institute of Technology, Thammasat University, Khlong Luang, Pathum Thani, 12120 Thailand*

Received: 31 August 2017; Revised: 2 March 2018; Accepted: 7 June 2018

Abstract

The aim of this study is to present an evaluation of the thermal load effects on the behavior of a concrete arch dam in Thailand. A Three-Dimensional Finite Element model for the thermal transient analysis was implemented to determine the thermal distribution in the dam body. Environmental conditions, such as reservoir water temperature at all depths, ambient temperature, and solar radiation were considered in the analysis. Then, structural analysis was conducted to evaluate deflections and stresses in the dam caused by the temperature profile. The thermal analysis results indicated that the upstream face is strongly affected by reservoir water temperature, while air temperature and sunlight mostly affect the downstream and crest faces. The solar radiation increases the concrete surface temperature by about 2 ℃ to 7 ℃ above the ambient temperature and causes nonuniform temperature distributions on the dam faces. Though prior literature shows significant effects of seasonal temperature variations on dam behavior, the structural analysis results in this paper show that the thermal loads contribute very little to the stresses and deflections of a dam in Thailand.

Keywords: arch dam, finite element, solar radiation, thermal analysis, crack

1. Introduction

Thermal transient analysis and evaluation of thermal effects on concrete arch dam behavior are of interest for dam safety. The loads that should be considered in the structural analysis of an arch dam are: self-weight of the dam, loads caused by hydrostatic pressure, uplift pressure, silt pressure, seismic loads, and thermal loads. Neglecting the initial cement hydration heat, only relevant at an early age, the thermal loads on an old arch dam are influenced by two factors, namely seasonal temperature variations and solar radiation affecting the exposed dam faces.

*Corresponding author
Email address: kiet.bui@oude.edu.vn

The reservoir water temperature plays an important role in determining the distribution of temperature in a concrete dam body. Zhu (1997) established an analytical formula, based on observations of deep reservoirs, in order to estimate the water temperature versus time at different water depths. This has been applied in the boundary conditions on the upstream face of a dam, for heat transfer analysis of concrete arch dams.

Solar radiation increases the temperature on the exposed faces of a dam. Solar radiation decreases the temperature load in winter, but increases it in summer. The amount of heat absorbed from exposed dam faces due to solar radiation depends on the slope, orientation of the dam faces, and the latitude (Federal Energy Regulatory Commission, 1999).

Jin, Chen, Wang, and Yang (2010) indicated that solar radiation mainly affected the temperature distribution on the faces directly contacting air, mostly on the downstream side of the dam, while the temperature distribution on the upstream

face was mainly affected by the reservoir water temperature. A nonuniform temperature distribution was observed on the downstream face of a dam due to variations in solar radiation and shading effects (Jin *et al.*, 2010; Mirzabozorg, Hariri-Ardebili, Shirkhan, & Seyed-Kolbadi, 2014; Santillán, Salete, Vicente, & Toledo, 2014).

A temperature gradient causes, via thermal expansion, significant tensile stresses, concentrated near the exposed surfaces of a dam, and may lead to fine cracks on these faces (Khanzaei, Abdulrazeg, Samali, & Ghaedi, 2015; Leger, Venturelli, & Bhattacharjee, 1993; Sheibany & Ghaemian, 2006).

Regarding other aspects, Matsuo, Nishiuchi, Kanazu, and Ueda (1999) found that joint opening of an arch dam in Japan significantly increased radial deflection in the winter from that in the summer, due to the temperature distribution change and the shrinking of concrete in winter.

In this study, the effects of the variations of reservoir water temperature corresponding to real water levels in the operational phase, air temperature, and solar radiation on exposed surfaces of the dam, on the temperature distribution in the dam body of a concrete arch dam in Thailand, are investigated. Their impacts on deflections and stresses in the dam were studied by establishing a Three-Dimensional Finite Element (FE) model using the commercial ANSYS software.

2. Materials and Methods

2.1 Thermal analysis of concrete arch dams

2.1.1 Thermal conduction

Concrete was assumed to have uniform and isotropic thermal properties. The governing heat conduction equation in a solid region, represented in the Cartesian coordinate system, is shown in Equation (1) (Holman, 2010).

$$k\left(\frac{\partial^2 T}{\partial x^2}+\frac{\partial^2 T}{\partial y^2}+\frac{\partial^2 T}{\partial z^2}\right)+Q=\rho C\frac{\partial T}{\partial t} \quad (1)$$

where k is thermal conductivity ($\mathrm{W/m^{\circ}C}$), ρ is density ($\mathrm{kg/m^3}$), C is specific heat ($\mathrm{J/kg^{\circ}C}$), T is temperature (°C), Q is the internal heat generation per unit volume ($\mathrm{W/m^3}$), and t is time (s).

In the case of an old concrete dam, heat generation no longer happens since cement hydration is already completed. So, the internal heat generation Q in Equation (1) can be neglected.

2.1.2 Thermal convection

The rate of interfacial heat convection is expressed by Newton's cooling law shown in Equation (2) (Holman, 2010).

$$q_c=h_c(T_s-T_a) \quad (2)$$

where h_c is convection coefficient ($\mathrm{W/m^2{\circ}C}$), T_a is surrounding air temperature (°C), and T_s is the temperature at the concrete face (°C).

There are some empirical formulas to determine the value of the air convection coefficient. The one proposed by Duffie and Beckman (2013) is shown in Equation (3).

$$h_{c-a}=5.7+3.8V \quad (3)$$

where h_{c-a} is the air convection coefficient at the dam face ($\mathrm{W/m^2{\circ}C}$), and V is wind speed (m/s).

2.1.3 Solar radiation

Heat flux caused by the solar radiation impacting a dam face depends on the absorptivity of the concrete, terrain factor, and orientation of the dam. The amount of heat absorbed by the concrete can be estimated as in Equation (4) (Leger *et al.*, 1993).

$$q_a=\delta R_t \quad (4)$$

where R_t is the global radiation intensity affecting the exposed face ($\mathrm{W/m^2}$), and δ is solar absorptivity coefficient. Typical δ of a concrete material is in the range 0.5–0.7 (Branco & Mendes, 1993; Larsson & Thelandersson, 2011; Saetta, Scotta, & Vitaliani, 1995).

In addition, the thermal radiation exchange between the concrete face and the surrounding environment, these being at different temperatures, is assessed by the Stefan- Boltzmann law shown in Equation (5) (Holman, 2010).

$$q_r=e\sigma(T_s^4-T_a^4) \quad (5)$$

where T_s is concrete surface temperature (°C), T_a is ambient temperature (°C), $\sigma=5.669\times10^{-8}$ is the Stefan-Boltzmann constant ($\mathrm{W/m^2K^2}$), and e is the emissivity coefficient. Typical e values used for concrete materials vary in the range 0.65–0.90 (Saetta *et al.*, 1995; Sheibany & Ghaemian, 2006).

2.1.4 Boundary conditions

The environmental conditions for an arch dam and the heat transfer mechanisms utilized in the analysis are shown in Figure 1.

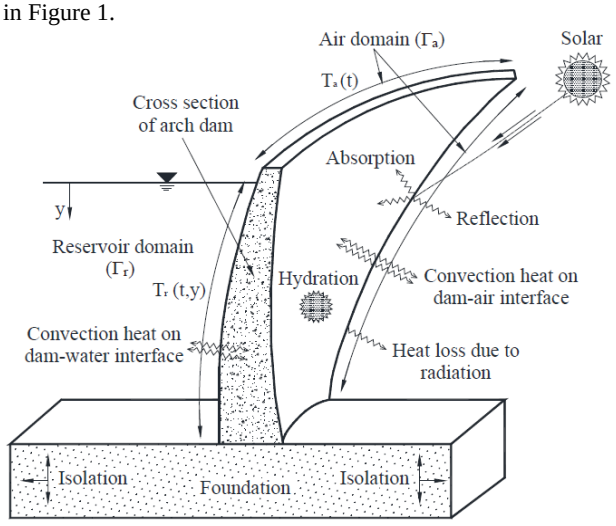

Figure 1. Heat transfer mechanisms of an arch dam.

The applied boundary conditions to solve Equation (1) are given in Equations (6) and (7) below.

$$k\left(\frac{\partial T}{\partial x}n_x + \frac{\partial T}{\partial y}n_y + \frac{\partial T}{\partial z}n_z\right) = q_a + q_{c-a} + q_r$$
on the air domain $\mathbf{\Gamma}_a$ (6)

$$k\left(\frac{\partial T}{\partial x}n_x + \frac{\partial T}{\partial y}n_y + \frac{\partial T}{\partial z}n_z\right) = q_{c-r}$$
on the water domain $\mathbf{\Gamma}_r$ (7)

where q_a is heat absorbed by concrete surfaces (W/m^2); q_{c-a} and q_{c-r} are convection heat on the concrete-air interface and concrete-water interface (W/m^2), respectively; q_r is thermal radiation emitted by the concrete body (W/m^2); n_x, n_y, and n_z are x, y, and z components of the surface normal and the position vector components, respectively; an $\mathbf{\Gamma}_a$ and $\mathbf{\Gamma}_r$ are air domain and reservoir water domain, respectively.

2.2 Numerical model of the dam

2.2.1 Dam description

The dam is located at 17^{0}14.55' latitude and 98^{0}58.33' longitude on the Ping River in Tak province, Thailand. It was constructed in the period of 1958-1964. The dam is considered as a moderately thin arch dam (U.S Army Corps. of Engineers, 1994). The main characteristics of the dam are shown in Table 1, and Figure 2a shows the overall dimensions of the dam.

Table 1. Main characteristics of the dam.

Characteristic	Unit	Value
Maximum dam height	m	150.0
Crest elevation above mean sea level (amsl)	m	261.0
Crest thickness	m	6.0
Base thickness at the central block	m	44.0
Number of concrete blocks of dam divided by contraction joints	-	25.0
Arch length at crest elevation	m	486.0
Arch radius	m	250.0
Normal water level (NWL) amsl	m	260.0
Minimum water level amsl	m	213.0
Reservoir capacity at NWL	m^3	13.5×10^9

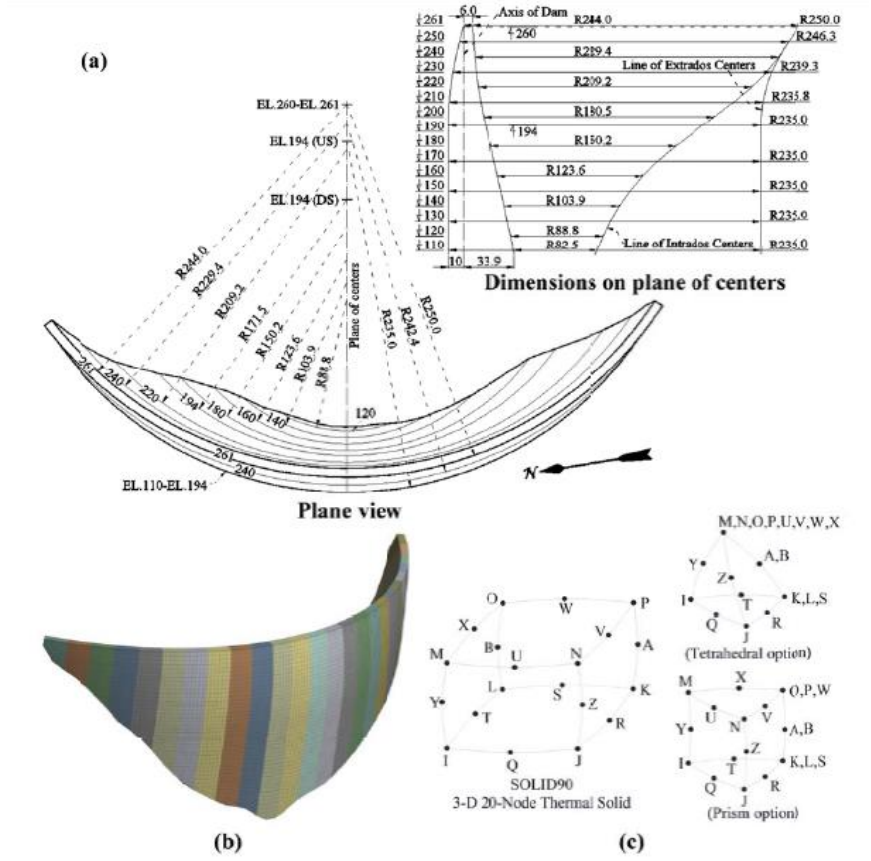

Figure 2. Basic dimensions and finite element meshing of the dam: (a) Basic dimensions, (b) Finite element meshing, (c) 3-D Thermal Elements.

2.2.2 Establishing 3-D thermal finite element model

A 3-D thermal FE model of the dam was implemented for thermal transient analysis. The meshing of the thermal FE model for the dam is shown in Figure 2b.

SOLID90 elements (42,636) were used. They include 3 layers at the crest and 18 layers at the base in the direction of the dam thickness. The elements have 20 nodes with one thermal degree of freedom at each node (Figure 2c). Due to the complex shape of the dam base, other element types (i.e. 10-node tetrahedral option, 15-node prism option) were used at bottom edges of the upstream and downstream faces. Contraction joints were modeled by using CONTACT174 and TARGET 170 elements with the bonded contact option.

2.2.3 Input data for the model

Environment conditions such as water temperature versus time at different depths, air temperature versus time, and solar radiation versus time were used as boundary conditions in the thermal transient analysis.

1) Reservoir water temperature

Based on a large amount of observations of water temperature in deep reservoirs, the experimental–analytical formula proposed by Zhu (1997) was used to calculate the water temperature, which varies with depths and seasons. Local climate conditions were considered, and modifications of the frequency ω of temperature variations in Zhu's equation were made to fit the tropical climate of Thailand.

The water temperature of the dam reservoir was determined from Equation 8.

$$T(y,t) = T_m(y) + A_y \cos\omega(t - t_0 - \varepsilon) \quad (8)$$

where $T(y,t)$ is the reservoir water temperature (℃) versus time t (day) at depth y (m), $T_m(y)$ is mean annual temperature of the water (℃), A_y is the amplitude of annual variations of water temperature (℃), ω is the frequency of temperature variations, t_0 is the time of maximum air temperature (day), and ε is the phase difference between the maximum temperature of water and air (day).

The mean annual temperature $T_m(y)$ is determined from Equation 9:

$$T_m(y) = C + (T_s - C)e^{-0.04y} \quad (9)$$

The parameter C is a function of annual temperature of reservoir water at the surface and bottom, as here:

$$C = \frac{(T_b - e^{-0.04H}T_s)}{(1 - e^{-0.04H})} \quad (10)$$

where T_s (℃) and T_b (℃) are the mean annual temperature of the reservoir water at the surface and at the bottom, respectively, and H (m) is the reservoir depth.

The amplitude of annual variations of reservoir water temperature $A(y)$ can be obtained from Equation 11.

$$A(y) = \left(\frac{T_{\max} - T_{\min}}{2}\right) e^{-\beta_0 y} \quad (11)$$

where $T_{\max}$(℃) and $T_{\min}$(℃) are maximum and minimum monthly mean air temperatures, respectively, and β_0 is a function of reservoir depth.

The parameter β_0 is a function of reservoir depth and is determined from Equation 12:

$$\beta_0 = \max(0.018, -0.058545 + 7.2727 \times 10^{-4} \times H) \quad (12)$$

The parameter ε is the phase difference between the maximum temperatures of water and air, as shown in Equation 13.

$$\varepsilon = 2.15 - 1.3e^{-0.085y} \quad (13)$$

Variations of water level of the reservoir during 2011-2013 were recorded by the Electricity Generating Authority of Thailand (EGAT). Since the operational water level is not constant, but varies with time, the input data of the water temperature along the depth, which is used to define the convection on the upstream dam surface below the free water surface, is processed in such a way that its value is assumed to be constant for each ten meters of water depth. Then, the operational water level of the reservoir is approximated, as shown in Figure 3a.

The mean daily air temperature and water temperature in 2013 of the reservoir are shown in Figure 5b as an example. As can be seen, large fluctuations of water temperature mainly occur in the upper part of the reservoir (from the free water surface to a depth of 15 m below the free surface) while the temperature of the lower part below a depth of 50 m is almost unchanged. In addition, the calculated results show a good correlation between air temperature and water temperature at different depths, as shown in Figure 3b.

2) Ambient temperature

The measured hourly air temperature history during 2011-2013 at a weather station near the dam site, supplied by Thai Meteorological Department (TMD), was used in the model. The ambient temperature was 11.5℃ – 40.8℃, as shown in Figure 4a.

3) Effects of solar radiation

Hourly global radiation data, collected at the Bangkok station, was used in the analysis. According to the orientation of the dam, which is in a North-South direction, the effects of solar radiation were separately considered for downstream face, crest, and upstream face above the reservoir water level. Variations of global solar radiation during 2011-2013, supplied by the Thai Meteorological Department, and the influence of solar radiation on the dam faces, are shown in Figure 4b-c. The behavior shown in Figure 4c also matches on site observations by the authors.

2.2.4 Initial temperature

The dam is more than 50 years old with no thermal instrumentation in the dam body. No information of the initial temperature field in the dam body could be determined. Therefore, in order to perform thermal transient analysis, a

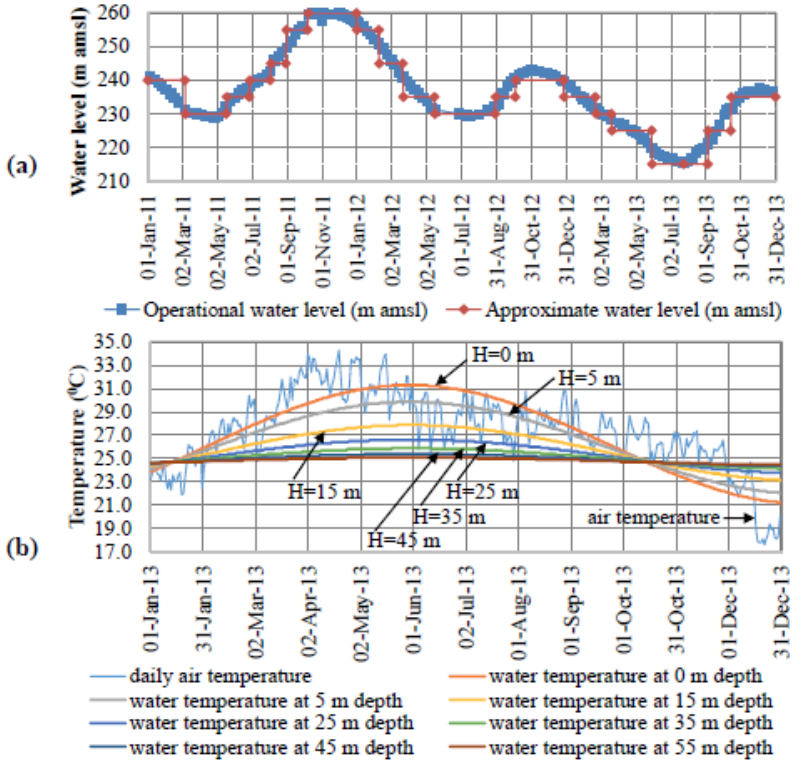

Figure 3. Variations of water level and calculated water temperature of the reservoir: (a) Variations of water level during 2011-2013, (b) Calculated water temperature in 2013.

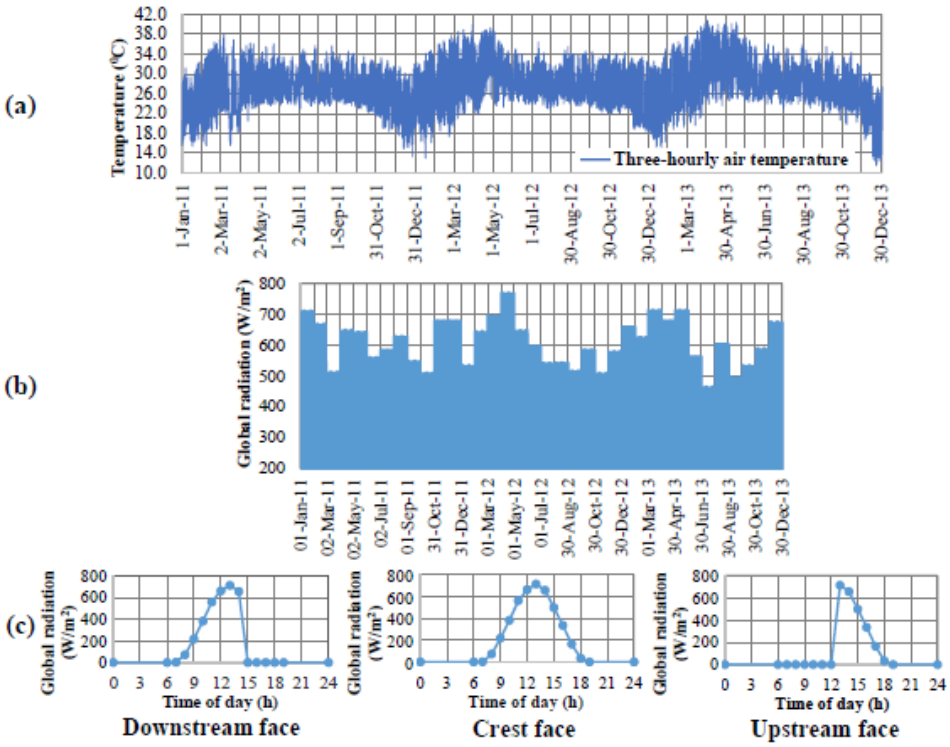

Figure 4. Hourly air temperature history at dam site and solar radiation during 2011-2013: (a) Hourly air temperature, (b) Solar radiation, (c) Example of typical hourly heat flux affecting on dam surfaces.

uniform temperature of 25℃ was assigned to all nodes initially. Then, the analysis was conducted for a period of 3 years (2011-2013) corresponding to the reservoir water level, which varied from a maximum depth of 149 m (at level of 260.0 m amsl) (above mean sea level) to a minimum depth of 104.4 m (at level of 215.4 m amsl).

In other words, there were 1096 steps with an hourly substep defined for the thermal transient analysis, to consider the effects of the variations of the environmental conditions such as water temperature, air temperature, and solar radiation. The analysis was repeated by applying the temperature field in the dam body at the end of each previous step as the new initial temperature value for the next step. This process was carried out several times until a stable thermal distribution in the dam body was achieved. The procedure to determine the real initial temperature condition is described in Figure 5.

2.2.5 Thermal properties and other significant parameters

The concrete thermal properties of the dam in the model, such as thermal conductivity and specific heat, were collected from a technical report (Bureau of Reclamation, 1963), while other concrete structural properties, such as density, modulus of elasticity, and Poisson's ratio were obtained from field tests. The thermal properties of the dam concrete and other important properties used in the study are presented in Table 2.

The dam-water convection coefficient is a variable in the range 0-6000 (Hariri-Ardebili, Shirkhan, & Seyed-Kolbadi, 2014). This coefficient is selected based on its minimum value that would give the same temperature for the concrete surface and the water in contact with it. The convection coefficient value of 340 (Table 2) is high enough to take into account the balance of temperature between water and concrete surface.

Table 2. Thermal and other properties used in the analysis.

Parameter	Symbol	Unit	Value
Thermal conductivity	k	W/m℃	2.72
Specific heat	C	J/kg℃	983
Density	ρ	kg/m^3	2480
Static modulus elasticity	E	GPa	44.18
Poisson's ratio	υ	-	0.228
Static compressive strength	f_c'	MPa	51.29
Static tensile strength	f_t	MPa	3.077
Dam-air convection coefficient	$h_{c\text{-}a}$	W/m^2℃	14[(a)]
Dam-water convection coefficient	$h_{c\text{-}w}$	W/m^2℃	Variable (340)[(b)]
Emissivity coefficient	e	-	0.65–0.90 (0.88)[(b)]
Solar absorptivity coefficient	δ	-	0.50–0.70 (0.60)[(b)]

[(a)] For an assumed average annual wind speed of 2.2 m/s.
[(b)] In the parentheses are the values of dam-water convection coefficient, emissivity coefficient, and solar absorptivity coefficient that were used in the analysis.

3. Results and Discussion

3.1 Thermal transient analysis

Transient thermal analysis was conducted for 3 years, from 2011 to 2013, with an hourly time step. The location of block 12, used for reporting analytical results as an example and the nodes of interest at block 12, are shown in Figure 6a.

Results from the FE model indicate that the nodes at the downstream face, such as node No. 8, are strongly affected by ambient temperature, as can be seen in Figure 6b. The temperatures of nodes No. 3 and No. 13 show the same trend as node No. 8, as they are all located on the downstream face. Furthermore, the temperature at this node is always higher than the ambient temperature due to absorption of solar radiation, as shown in Figure 6b. In addition, the temperatures at other nodes on the upstream face, such as nodes No. 4, No. 9, and No. 14, are mainly affected by the reservoir water temperature as shown in Figures 9c-e.

Node No. 2 at the upper level is more significantly influenced by the environmental conditions than inner nodes at lower levels, such as node No. 6 at level 200.0 m amsl (Figure 6c) or node No. 11 at level 150.0 m amsl (Figure 6d), or node No. 16 at level 125.0 m amsl (Figure 6e).

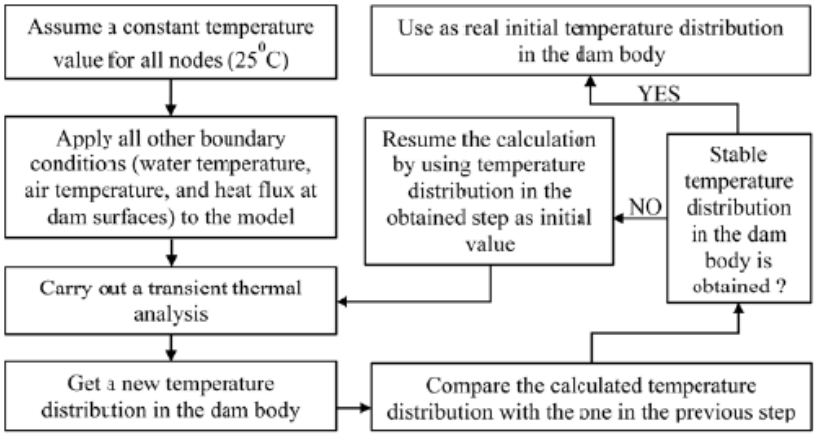

Figure 5. Procedure to determine the initial temperature condition.

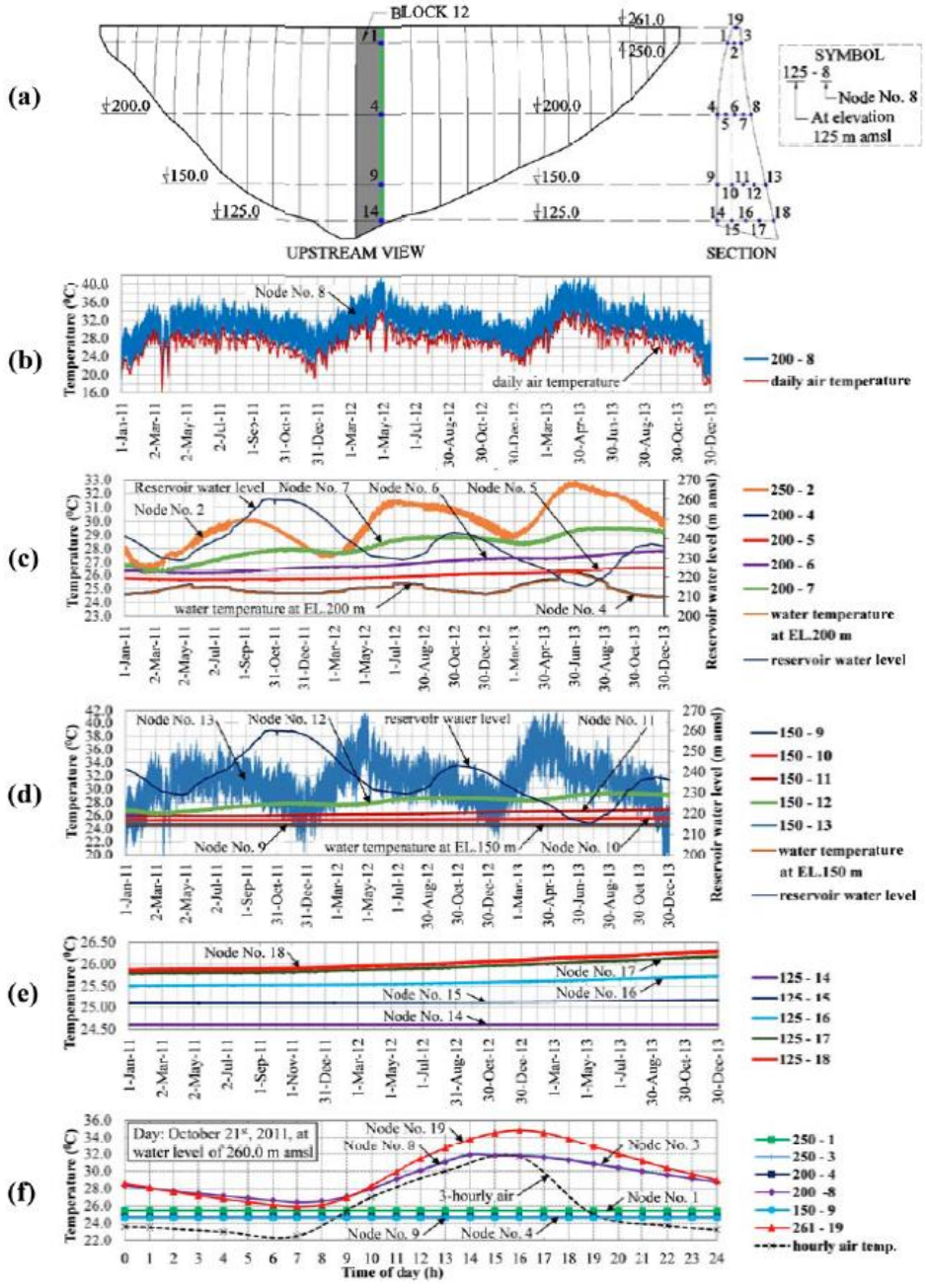

Figure 6. Temperature variations at nodes: (a) Location of nodes of interest at block 12, (b) node No. 8 at downstream face, (c) nodes at upper levels, (d) nodes at middle level, (e) nodes at lower level, and (f) boundary nodes at dam surfaces.

When taking the effects of solar radiation into consideration, Figure 6f shows that the temperatures at nodes No. 3 and No. 8 on the downstream face, and node No. 19 on the crest face were about 2 ℃ to 7 ℃ higher than the air temperature at the same time. The temperature at node No. 19 on the crest is also higher than others (i.e. nodes No. 3 and No. 8) at the downstream face, because of the higher heat flux received from the sun. The nodes No. 1, No. 4, No. 9 and No. 14 at the upstream face, which are submerged in the reservoir water, are not subjected to solar radiation but are strongly affected by the reservoir water temperature and fluctuations of water level (Figures 6c-f). Also, at depths deeper than 50 m from the free water surface, the temperature at the upstream face is almost unchanged, as can be observed from the temperatures at node No. 9 (Figure 6d) and node No. 14 (Figure 6e).

Federal Energy Regulatory Commission (1999) introduced a reasonable approximation for a sufficiently thin arch dam from reservoir water temperature on the upstream face to ambient temperature on the downstream face, using a simplified method. In this case, a linear distribution of temperature along the dam thickness of the dam body may be

assumed. In this study, the type of dam is classified as a moderately thin arch dam with varying arch dam thickness along the dam axis (Figure 2a). In addition, the reservoir water level, water temperature, air temperature, and also solar radiation were considered as factors that vary with time. Hence, the temperature distribution in the dam body is nonlinear along the dam thickness.

Besides, the air temperature during night time is low but concrete surface received heat from adjacent internal concrete parts of the dam body. So the temperature at the concrete surface cooled down slower than the air temperature at night (Figure 6f).

The temperature distributions on the dam faces for 2012, corresponding to the fluctuations of water level, are shown in Figure 7.

Figure 7 indicates that the solar radiation, increasing temperatures at the exposed faces, is not uniform due to the orientation of the dam. For instance, the durations of daily heat flux affecting the dam crest face, downstream face, and upstream face are 12, 7, and 7 hours, respectively (Figure 4c). As a result, the temperature of the crest face is higher than that of the others. In addition, the maximum differential temperature between inner nodes (i.e. node No. 6 and No. 11) and nodes at the surfaces (i.e. node No.8 and No.13, respectively) is about 16℃. Therefore, there is no possibility of cracking caused by thermal load, as can be proven by the thermal stress analysis in the next section.

To validate the thermal analysis results in this study, field measurements were conducted in May 2017 by using an infrared camera to measure the concrete surface temperatures. The temperature difference between air and concrete surface was about 4.8 ℃ at the upstream face and 6.9 ℃ at the downstream face. These data from field measurements were in good agreement with the FEM analysis results.

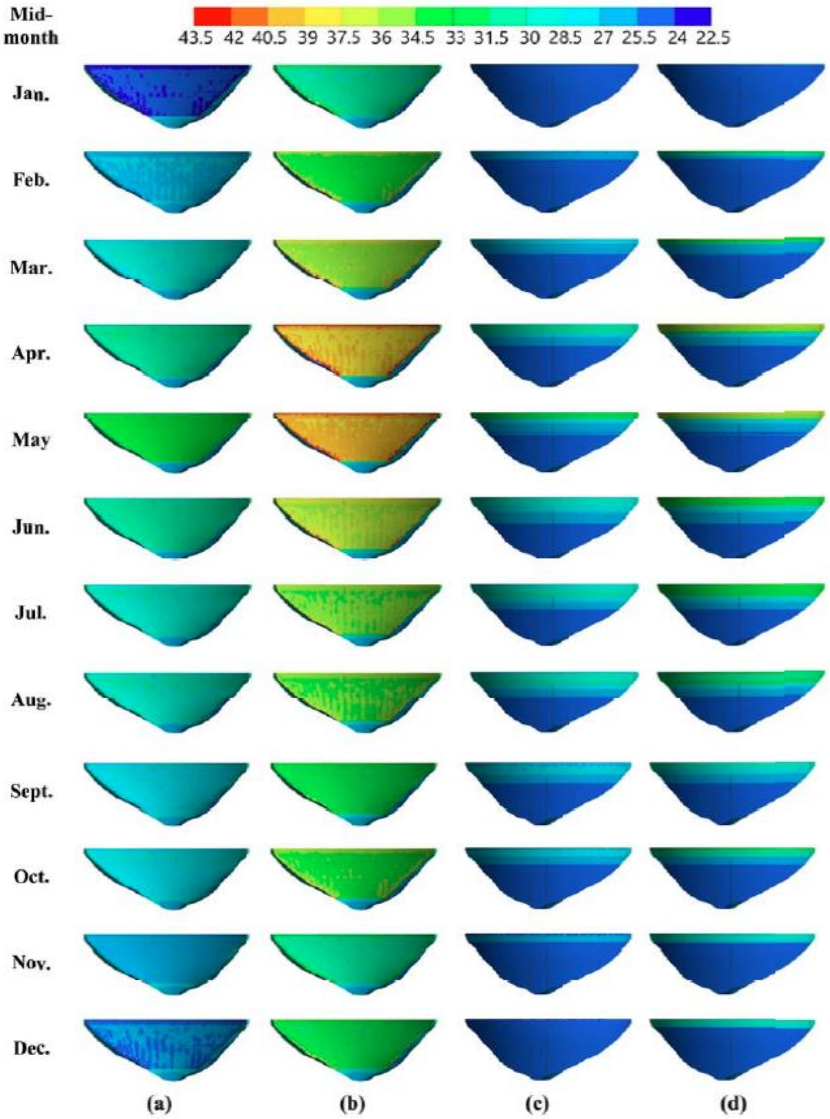

Figure 7. Distribution of temperature (℃) on downstream face at (a) 8:00 am, (b) 2:00 pm, and upstream face at (c) 8:00 am, (d) 2:00 pm.

3.2 Structural analysis

The temperature distribution in the dam body, obtained from the thermal transient analysis, was used as the thermal load on the dam. To evaluate the effects due to temperature load, the analysis was conducted by considering only the temperature effects in the linear structural analysis for two cases, corresponding to a day in the hottest month (April 2012) and a day in the coldest month (December 2011). The deformation of the dam in the stream direction and stress distribution in the dam body, caused by temperature load only, are shown in Figure 8a-b.

Figure 8a shows that the temperature load has an insignificant effect on the deformation of the dam. Its value in the stream direction is in the range of -7.9×10^{-10} to 5.0×10^{-11} m. Besides, the FEM analysis results also indicate that there is only a small tensile stress on the dam surfaces, with its maximum 0.2 Pa near the dam base of the downstream surface, as shown in Figure 8b. These values are insignificant compared to the tensile strength of concrete (Table 2). Hence, thermal cracks are not possible on the dam surfaces, which agrees with observations of the dam faces by the dam maintenance engineers.

In past studies significant tensile stress concentrations near exposed surfaces have been caused by larger temperature gradients. The variations of mean daily water temperature and mean monthly air temperature in different seasons were about 29℃ and 26.5℃, respectively, (Sheibany & Ghaemian, 2006) or 22℃ and 19℃, respectively (Khanzaei, Abdulrazeg, Samali, & Ghaedi, 2015). In the present study, the smaller variations of daily water temperature and monthly air temperature were about 10℃ and 11.5℃, respectively, in the tropical climate of Thailand (Figures 3b, 6b). For this reason, tensile stress concentrations near the exposed surfaces were smaller than in prior studies.

In addition, the measurements by plumb line equipment installed in the dam body also confirm that displacements in the dam are mostly affected by the water level and self-weight of the dam, while the effects of temperature loads are small. Figure 8c shows the actual deflection of the dam recorded from plumb line when the operational water level of the reservoir is about 260 m amsl. It should be noted that the values of stream (radial) deflections shown in Figure 8c are the deflections relative to that at the water level 230 m amsl.

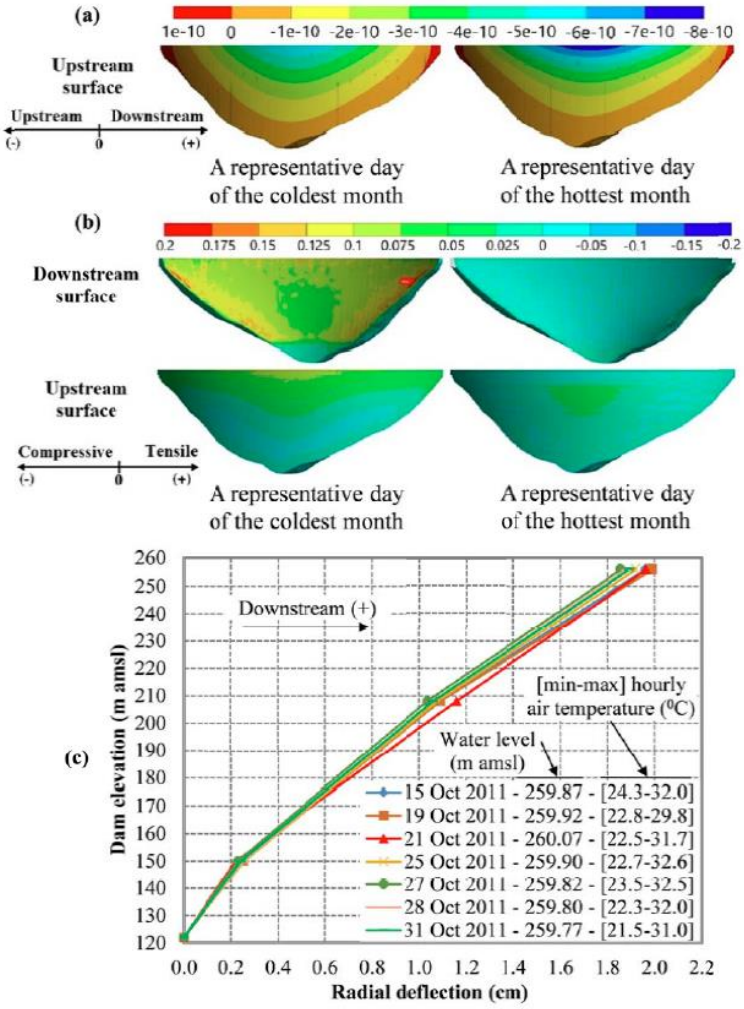

Figure 8. Deformation and stress distribution of the dam: (a) Deformation (m) in stream direction, (b) Maximum principal stress distribution (Pa), (c) Relative deflection (cm) measured by plumb line equipment.

4. Conclusions

Thermal transient analysis of a dam was conducted in this paper with consideration of the effects of real environmental conditions, including varied water temperatures at different depths, ambient temperatures collected from a weather station near the dam site, and hourly solar radiation. According to the results of the analysis, the conclusions can be summarized as follows:

1) The temperature distribution indicates that the downstream face, crest, and the part above the water level on the upstream face are mainly affected by the ambient temperature and sunlight, as they follow the variations of the ambient temperature and solar radiation.
2) Considering the solar radiation effects, the temperature of the concrete faces is 2℃ to 7℃ higher than the air temperature and the temperatures vary by face of the dam.
3) The upstream face submerged in water is mainly affected by the temperature of the reservoir water. At the lower part of the reservoir (depths deeper than 50 m), the temperature of the dam face is almost constant.
4) Due to the small temperature variations in the tropical climate of Thailand, the thermally generated tensile stresses are small and do not cause thermal cracking on the dam faces, which agrees well with observations of the dam faces.

The temperature field collected from the thermal transient analysis will be applied as temperature loads to analyze the total static and dynamic behavior of the dam in a future study.

Acknowledgements

The authors would like to acknowledge the Center of Excellence in Material Science, Construction and Maintenance Technology Project, Thammasat University, and the Electricity Generating Authority of Thailand for supporting this study.

References

Branco, F. A., & Mendes, P. A. (1993). Thermal actions for concrete bridge design. *Journal of Structural Engineering, 119*(8), 2313-2331.

Bureau of Reclamation, Department of the Interior, United States. (1963). *Concrete mix investigation - Bhumibol Dam - Yanhee project, Thailand - Concrete and structural report* (No. C-1055).

Duffie, J. A., & Beckman, W. A. (2013). *Solar engineering of thermal processes*. Hoboken, NJ: John Wiley and Sons.

Federal Energy Regulatory Commission. (1999). *Engineering guidelines for the evaluation of hydropower projects. Chapter 11-Arch Dams*. Washington, D.C.: Author.

Holman, J. (2010). *Heat transfer* (10th ed.). New York, NY: Mc-Graw-Hill.

Jin, F., Chen, Z., Wang, J., & Yang, J. (2010). Practical procedure for predicting non-uniform temperature on the exposed face of arch dams. *Applied Thermal Engineering, 30*(14), 2146-2156. doi:10.1016/j.applthermaleng.2010.05.027.

Khanzaei, P., Abdulrazeg, A. A., Samali, B., & Ghaedi, K. (2015). Thermal and structural response of RCC dams during their service life. *Journal of Thermal Stresses, 38*(6), 591-609. doi:10.1080/01495739.2015.1015862.

Larsson, O., & Thelandersson, S. (2011). Estimating extreme values of thermal gradients in concrete structures. *Materials and Structures, 44*(8), 1491-1500. doi:10.1617/s11527-011-9714-0.

Leger, P., Venturelli, J., & Bhattacharjee, S. (1993). Seasonal temperature and stress distributions in concrete gravity dams. Part 2: Behaviour. *Canadian Journal of Civil Engineering, 20*(6), 1018-1029. doi:10.1139/l93-132.

Matsuo, T., Nishiuchi, T., Kanazu, T., & Ueda, M. (1999). Investigation on the static behavior of an aged arch dam based on in-situ test results (in Japanese). *Journal of Japan Society of Dam Engineers, 9*(1), 4-12. doi:10.11315/jsde1991.9.4

Mirzabozorg, H., Hariri-Ardebili, M., Shirkhan, M., & Seyed-Kolbadi, S. (2014). Mathematical modeling and numerical analysis of thermal distribution in arch dams considering solar radiation effect. *The Scientific World Journal, 2014*. doi: 10.1155/2014/597393

Saetta, A., Scotta, R., & Vitaliani, R. (1995). Stress analysis of concrete structures subjected to variable thermal loads. *Journal of Structural Engineering, 121*(3), 446-457.

Santillán, D., Salete, E., Vicente, D., & Toledo, M. (2014). Treatment of solar radiation by spatial and temporal discretization for modeling the thermal response of arch dams. *Journal of Engineering Mechanics, 140*(11), 05014001. doi:10.1061/(ASCE)EM.1943-7889.0000801.

Sheibany, F., & Ghaemian, M. (2006). Effects of environmental action on thermal stress analysis of Karaj concrete arch dam. *Journal of Engineering Mechanics, 132*(5), 532-544. doi:10.1061/(ASCE)0733-9399(2006)132:5(532).

United States Army Corps of Engineers (1994). *Engineering and design - Arch dam design. Engineer manual 1110-2-2201*. Washington, D.C.: Author.

Zhu, B. (1997). Prediction of water temperature in deep reservoirs. *Dam Engineering, 8*, 13-25.